Univerza
v Ljubljani
Fakulteta
za gradbeništvo
in geodezijo

Jamova 2
1000 Ljubljana, Slovenija
http://www3.fgg.uni-lj.si/

DRUGG – Digitalni repozitorij UL FGG
http://drugg.fgg.uni-lj.si/

University
of Ljubljana
Faculty of
Civil and Geodetic
Engineering

Jamova 2
SI – 1000 Ljubljana, Slovenia
http://www3.fgg.uni-lj.si/

DRUGG – The Digital Repository
http://drugg.fgg.uni-lj.si/

Efficient handling of stability problems in shell optimization by asymmetric 'worst-case' shape imperfection

M. Kegl[a], B. Brank[b], B. Harl[a], M.M. Oblak[a]

[a]*Faculty of Mechanical Engineering, University of Maribor, Smetanova 17, 2000 Maribor, Slovenia*
[b]*Faculty of Civil and Geodetic Engineering, University of Ljubljana, Jamova 2, 1000 Ljubljana, Slovenia*

ADDRESS:
M. Kegl
FACULTY OF MECHANICAL ENGINEERING
Smetanova 17
SI-2000 Maribor
SLOVENIA
Telephone: (+386 2) 220-7802
Telefax: (+386 2) 220-7990
E-mail: marko.kegl@uni-mb.si

Abstract

The paper presents an approach to shape optimization of stability-sensitive elastic shell structures with conservative proportional loading. To reduce the stability-related problems, a special technique is utilized, by which the response analysis is always terminated before the first critical point is reached. In that way, the optimization is always related to a pre-critical structural state. The necessary load-carrying capability of the optimal structure is assured by extending the usual formulation of the optimization problem by a constraint on an estimated critical load factor. Since limit points are easier to handle, the possible presence of bifurcation points is avoided by introducing imperfection parameters. They are related to an asymmetric shape perturbation of the structure. During the optimization, the imperfection parameters are updated to get automatically the 'worst-case' pattern and amplitude of the imperfection. Both, the imperfection parameters and the design variables are related to the structural shape via the design element technique. A gradient-based optimizer is employed to solve the optimization problem. Three examples illustrate the proposed approach.

KEYWORDS: Structures; Optimization; Stability; Shells; Shape design; Imperfection

1. Introduction

Optimization of statically loaded elastic structures has become an integral part of many modern design procedures. Optimization of linear structures is now well established, however, this still can not be said for optimization of structures with geometrically nonlinear behaviour. Namely, by introducing geometrical nonlinearity into optimization, one is confronted with the following difficult tasks: *(i)* The *instability phenomena* has to be dealt with due to possible presence of critical points on the equilibrium path. Early works addressing this problem go back to 1980s, References [1,2], and since then a considerable effort has been invested into addressing the related issues, see e.g. References [3-9]. *(ii)* The *sensitivity analysis of critical point* quantities has to be performed, see e.g. References [10-15]. The computation of sensitivities can be rather difficult, if the first critical point is a bifurcation point. *(iii)* Initial *geometric imperfections* have to be considered to calculate a reliable critical load of a real structure and to include imperfections into the optimization process. This is especially important for shell structures, for which the critical load factors may be extremely reduced by imperfections, see e.g. Reference [16].

A typical approach in optimization of stability-sensitive structure is to introduce the critical load factor of a geometrically perfect (or imperfect) structure into the definition of the optimization problem; the term *stability-sensitive structure* is used here for a perfect or an imperfect structure, with at least one critical point on its equilibrium path. Obviously, this is the most natural choice since it enables optimization with objectives or constraints, explicitly defined in terms of the critical state quantities. Its drawback is a substantial increase of complexity of the structural response and sensitivity analysis (see e.g. Reference [15] for a brief review on those issues). Namely, if constraints on displacements or stresses are also part of the optimization problem, two types of structural analyses are typically needed: *(i)* The complete *nonlinear incremental* analysis to compute the displacements, stresses, etc. at the *full load level*, usually corresponding to a regular (but possibly post-critical) structural state. This analysis (here termed the *displacement analysis*) is typically based on the arc-length method. The corresponding sensitivity analysis is relatively straightforward. *(ii)* The *critical point* analysis to obtain the critical state quantities (usually the first critical point on the equilibrium path is of interest). An incremental approach may be used, but direct computation is also possible, see e.g. Reference [17] or [18]. The corresponding sensitivity analysis might be quite sophisticated, Reference [19].

In this work an alternative approach to optimization of stability-sensitive structures with geometric imperfections is proposed. Its basic ingredients can be outlined as:

(i)   Only the *displacements analysis* is utilized. The optimal design procedure is always related to a regular equilibrium point, preceding the first critical point.

(ii)   The critical load factor constraint is introduced in an approximate way, since the critical load factor and its sensitivity are obtained by an estimate.

(iii) The approach is computationally efficient, since the only extra computational cost, with respect to the optimal design of stability-insensitive structures, see e.g. Reference [20], is due to the estimation of the critical load factor. One eigenvalue and the corresponding eigenvector are computed at each structural equilibrium state.

(iv)   An asymmetric shape imperfection is introduced via the design element technique (also called the parametric curve/surface/body approach). Since the critical points of limit type usually occur in the analysis of imperfect structures, the critical points of bifurcation type are avoided. Surprisingly, this greatly simplifies the optimal design procedure.

(v)   The computation of the 'worst-case' imperfection is integrated into the iterative optimization procedure. In the first stage of optimization the imperfection pattern is found by a simple update procedure; then its norm (or amplitude) is determined.

In this paper, shell structures are addressed only. However, the proposed procedure is not limited to this type of structures.

The outline of the paper is as follows. Section 2 briefly describes the problems arising in optimization of geometrically nonlinear stability-sensitive structures. Section 3 describes the basic setup of the proposed approach, a procedure to avoid the bifurcation nature of the first critical point, and a procedure to obtain adequate pattern and amplitude of imperfection. In Section 4 three numerical examples are presented and discussed.

2. Problem description

A typical optimization problem of a statically loaded structure with nonlinear response (further called a nonlinear structure) may be stated as

$$\min f_0$$
$$s.t. \quad f_i \le 0, \quad i = 1, \ldots, M \tag{1}$$

where $f_0 = f_0(\mathbf{b}, \mathbf{u})$ and $f_i = f_i(\mathbf{b}, \mathbf{u})$ are objective and constraint functions, respectively. The constraint functions are typically related to displacements, stresses, etc. The symbol $\mathbf{b}$ denotes the vector of design variables and $\mathbf{u}$ is the vector of response variables, usually displacements and rotations of the structural model, discretized by finite elements. Implicit dependence of $\mathbf{u}$ on $\mathbf{b}$ is given through the structural equilibrium equation, which can be written as

$$\mathbf{F} - \lambda \mathbf{R} = \mathbf{0} \tag{2}$$

For elastic and conservative structures, Equation (2) is obtained from the stationary condition of the potential energy, discretized by finite elements. Here $\mathbf{F} = \mathbf{F}(\mathbf{b}, \mathbf{u}^\lambda)$ and $\lambda \mathbf{R} = \lambda \mathbf{R}(\mathbf{b})$, where $\mathbf{u}^\lambda = \mathbf{u}(\lambda)$, are the vectors of internal and external (load) forces of the discretized structural model. Proportional loading is assumed in Equation (2) with λ representing the load factor, $0 \le \lambda \le 1$. The response vector $\mathbf{u}$ is related to full load level $\lambda = 1$, i.e. $\mathbf{u} = \mathbf{u}^{\lambda=1}$.

The optimization problem (1) is often solved by utilizing gradient-based optimization methods. The solution procedure is iterative. Each iteration requires at least one response analysis (i.e. solution of Equation (2) for $\mathbf{u}$ at some fixed $\mathbf{b}$) along with the corresponding sensitivity analysis, and one call of a gradient-based optimization algorithm, which calculates the improved design variables $\mathbf{b}$. The displacement analysis is performed by an incremental process, where λ is gradually increased until the final load factor $\lambda = 1$ is reached. The obtained curve in the $\lambda - \mathbf{u}^\lambda$ space is called the equilibrium path. While incrementing λ, the equilibrium path of a nonlinear structure may reach a critical point, located at some critical load factor λ^c. In that case, the structure buckles before it is completely loaded.

If a critical point is encountered on the equilibrium path, the optimization process will most probably not be able to deliver the solution of the optimization problem (1). The response analysis may break due to convergence problems, if the path-following methods like the arc-length method, see e.g. Reference [21], are not used in conjunction with Equation (2). But even if an adequate response analysis technique is utilized, the optimization process will probably produce an alternating sequence of stable, $\lambda^c > 1$, and unstable, $\lambda^c < 1$, design solutions. The chances to get an acceptable solution are rather minor.

To suppress the stability-related problems, the most natural choice seems to be an

introduction of a constraint on the critical load factor λ^c, i.e. by adding

$$\lambda^c \geq 1 \qquad (3)$$

to Equations (1). Indeed, doing so proves to be helpful, as shown e.g. in Reference [15], but one might have serious concerns about the effectiveness of such an approach. The first important drawback is related to the fact that now one has to perform two types of structural response analysis: the displacement analysis to get $\mathbf{u}$, and the critical point analysis to get λ^c. Of course, adequate sensitivity analyses are also needed. The sensitivity analysis of a critical load factor λ^c, which corresponds to a limit point, is rather straightforward, e.g. Reference [22]. In contrast, the sensitivity analysis of a critical load factor λ^c, related to a bifurcation point, is far more complicated, see e.g. Reference [19]. Therefore, one can conclude that by adding the critical load factor constraint (3) to Equations (1), the complexity of the structural response and sensitivity analysis will increase enormously. The same holds for the computational cost of the optimization process. The second major drawback is related to the path-following displacement analysis. An equilibrium path of a shell structure may contain numerous critical points, possibly many of them being bifurcation points. A conventional arc-length procedure may, after passing a bifurcation point, follow either the primary or the secondary equilibrium branch. It is thus possible that the final load factor, $\lambda = 1$, is reached only after an immense computational effort, as illustrated in Figure 1 for a case of a snow-loaded shell with hinged corners. The load factor diagram clearly shows that $\lambda = 1$ is reached only after computing more than 200 equilibrium states. In such situations, the computational effort for the displacement analysis may increase beyond all acceptable limits.
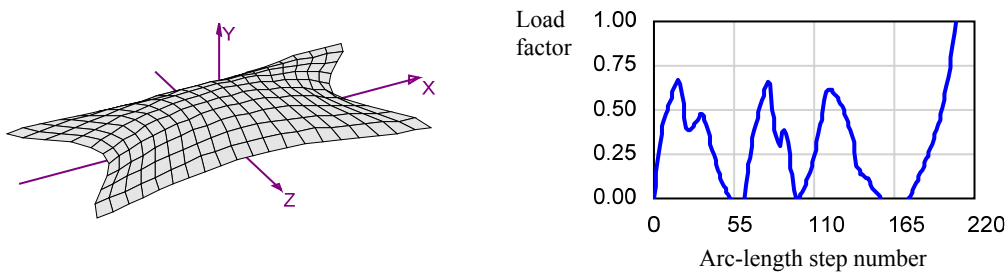

Figure 1. A snow-loaded shell and the corresponding load factor history.

One can see from the above that adding the critical load factor constraint (3) to Equations (1)

may not help to solve the optimization problem in a satisfactory manner. Even more, such an approach seems to be an inefficient and rather complicated option. For this reason, alternative formulations have been proposed in the past. For example, Wu and Arora [22] suggested to perform a usual optimization step, if the current design corresponded to a stable structure. In the opposite case, the critical load factor constraint was added to the optimization problem and the actual response **u** was assumed by approximating the final part of the equilibrium path as illustrated in Figure 2a. Such **u** was obviously not correct, but hopefully good enough to proceed successfully with the optimization process. The drawback of this approach is that it often leads to oscillations in the optimization process. Furthermore, the sensitivity analysis in Reference [22] is valid only for limit points; bifurcation points are not addressed.
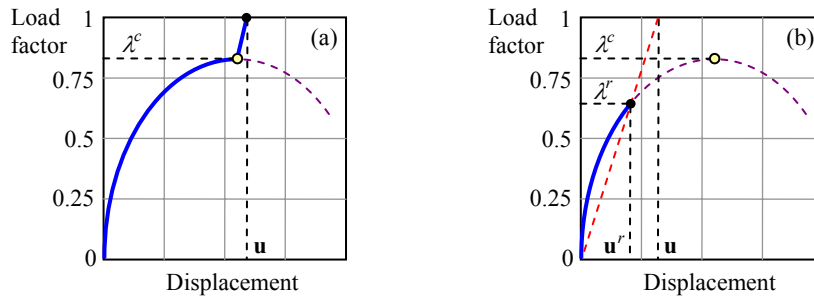

Figure 2. Alleviating stability problems: (a) equilibrium path modification and (b) response analysis termination before the critical load factor.

In contrast to Reference [22], the approach proposed in Reference [23] resulted in a more stable optimization process. The authors suggested to terminate the response analysis at some load factor λ^r, which is always lower than the critical load factor λ^c, Figure 2b. Before entering the optimization algorithm, the displacements $\mathbf{u}^r$ at λ^r were scaled by $1/\lambda^r$. A special procedure was employed to make sure that the final optimization steps were performed at $\lambda^r = 1$. In place of the actual critical load factor constraint (3), the constraint on some estimated critical load factor λ^* was utilized. Again, the proposed sensitivity expression for λ^* was valid only for limit points; bifurcation points were not addressed.

Initial imperfections very often play a crucial role in structural stability capacity. It is therefore important to include them into the optimal design process. The simplest way is to use a predefined imperfection shape (usually related to a buckling mode) and a predefined amplitude, and solve an optimization problem for a geometrically nonlinear structure, see e.g.

6

References [15] and [5]. Another way, which is considerably more demanding, was taken e.g. by Mroz and Piekarski [6], Ohsaki [24], Ohsaki et al.[25], who included imperfection parameters into the design process in order to get the 'worst' possible imperfection mode, i.e. the mode, which reduces the most the structural load-carrying capacity. Away from optimization, one may also mention the direct approach to evaluation of the 'worst' imperfections by introducing the imperfection nodal variables into the potential energy functional, see e.g. References [26] and [27]. In the present work, initial geometric imperfections are included into the optimization process, and a procedure is proposed to obtain the 'worst' pattern and amplitude of imperfections, along with the optimal design.

3. The proposed approach

3.1 Basic setup

Let us consider an elastic nonlinear shell structure, subjected to a proportional load and let the corresponding optimization problem be given by Equations (1). To alleviate possible stability problems, the original optimization problem (1) is modified as

$$
\begin{aligned}
&\min f_0^r \\
&s.t. \quad f_i^r \leq 0, \quad i = 1, \ldots, M \\
&\qquad \lambda^* \geq 1 + \beta
\end{aligned}
\tag{4}
$$

The superscript r in Equations (4) indicates that the quantity is computed at the structural equilibrium state, which corresponds to the load factor $\lambda^r \leq \min\left(1, \lambda^c - \varepsilon\right)$. Here ε is a small positive number, which assures that λ^r in not too close to λ^c since this might cause numerical problems. The symbol λ^* denotes an estimation of the critical load factor and β is some given constant, which can be seen as a desired safety of the structure against buckling.

The load factor λ^r is searched within the usual load-driven incremental displacement analysis as follows. At current equilibrium state $\mathbf{u}^n$, related to λ^n, an approximate critical load factor λ^* is computed. It is then checked whether λ^* is close to λ^n. If it is, λ^r is set equal to λ^n and the response analysis *is terminated*. Otherwise, the response analysis is continued to the next load factor $\lambda^{n+1} = \lambda^n + \Delta\lambda$, where $\Delta\lambda$ is a prescribed load factor increment. As a guideline, λ^* can be considered to be close to λ^n, if $\lambda^* \leq \lambda^n + \delta$. Note that

the constant δ has to be smaller than β; this assures gradual increase of λ^r through the optimization process, until $\lambda^r = 1$ is finally reached. It is our numerical experience that $\delta = \beta/2$ works fine.

To compute λ^*, the tangent stiffness matrices $\mathbf{K}^n$ and $\mathbf{K}^{n-1}$ at load factors λ^n and λ^{n-1}, respectively, are used. Approximations for the critical load factor and the corresponding critical stiffness matrix can be written as (see e.g. Reference [28], section 6.5.8)

$$\lambda^c \approx \lambda^* = \lambda^{n-1} + \alpha^* \left(\lambda^n - \lambda^{n-1} \right)$$
$$\mathbf{K}^c \approx \mathbf{K}^{n-1} + \alpha^* \left(\mathbf{K}^n - \mathbf{K}^{n-1} \right) \tag{5}$$

Here α^* is the lowest eigenvalue of the generalized eigenproblem

$$\mathbf{K}^{n-1}\mathbf{y} + \alpha \left(\mathbf{K}^n - \mathbf{K}^{n-1} \right)\mathbf{y} = \mathbf{0} \tag{6}$$

and $\mathbf{y}^*$ is the eigenvector that corresponds to α^*. Provided that the first critical point along the equilibrium path is a simple critical point, one can make the following classification: $\mathbf{y}^{*T}\mathbf{R} \neq 0 \rightarrow$ limit point, and $\mathbf{y}^{*T}\mathbf{R} = 0 \rightarrow$ bifurcation point.

Assume now that the current response analysis is terminated at $\lambda^r \leq \min\left(1, \lambda^c - \varepsilon\right)$. The corresponding response is $\mathbf{u}^r$. The functions f_0^r and f_i^r in Equations (4) are computed using the scaled response

$$\mathbf{u} = \frac{\mathbf{u}^r}{\lambda^r} \tag{7}$$

In other words, $\mathbf{u}^r$ is utilized to compute f_0^r and f_i^r, which are the estimates of f_0 and f_i at $\lambda = 1$. This assures that the actual displacement and stress constraints are approximated good enough to get a better design in the next optimization step.

The calculation of sensitivities $d\mathbf{u}^r/d\mathbf{b}$ is done by utilizing the usual discrete sensitivity equation

$$\mathbf{K}^r \frac{d\mathbf{u}^r}{d\mathbf{b}} = \lambda^r \frac{d\mathbf{R}}{d\mathbf{b}} - \frac{\partial \mathbf{F}^r}{\partial \mathbf{b}} \tag{8}$$

In Equation (8) $\mathbf{K}^r = \partial \mathbf{F}/\partial \mathbf{u}$ at $\mathbf{u} = \mathbf{u}^r$ and $\partial \mathbf{F}^r/\partial \mathbf{b} = \partial \mathbf{F}/\partial \mathbf{b}$ at $\mathbf{u} = \mathbf{u}^r$. According to Equation (7), the design derivatives of f_0^r and f_i^r are obtained by using the scaled derivatives

$$\frac{d\mathbf{u}}{d\mathbf{b}} = \frac{1}{\lambda^r}\frac{d\mathbf{u}^r}{d\mathbf{b}} \tag{9}$$

The calculation of sensitivities $d\lambda^*/d\mathbf{b}$ is based on the formula for sensitivities of the critical load factor, see e.g. Reference [22],

$$\frac{d\lambda^c}{d\mathbf{b}} = \frac{\mathbf{y}^{cT}\left(\dfrac{\partial\mathbf{F}^c}{\partial\mathbf{b}} - \lambda^c\dfrac{d\mathbf{R}}{d\mathbf{b}}\right)}{\mathbf{y}^{cT}\mathbf{R}} \tag{10}$$

By utilizing the approximations $\lambda^c \approx \lambda^*$, $\mathbf{y}^c \approx \mathbf{y}^*$, and

$$\frac{\partial\mathbf{F}^c}{\partial\mathbf{b}} \approx \frac{\partial\mathbf{F}^*}{\partial\mathbf{b}} = \frac{\partial\mathbf{F}^{n-1}}{\partial\mathbf{b}} + \alpha^*\left(\frac{\partial\mathbf{F}^n}{\partial\mathbf{b}} - \frac{\partial\mathbf{F}^{n-1}}{\partial\mathbf{b}}\right) \tag{11}$$

see Reference [29], one gets the approximate sensitivities for the critical load factor

$$\frac{d\lambda^*}{d\mathbf{b}} = \frac{\mathbf{y}^{*T}\left(\dfrac{\partial\mathbf{F}^*}{\partial\mathbf{b}} - \lambda^*\dfrac{d\mathbf{R}}{d\mathbf{b}}\right)}{\mathbf{y}^{*T}\mathbf{R}} \tag{12}$$

Equations (5)-(9) and (12) is all one needs to perform the response and sensitivity analysis for the optimization problem, defined by Equations (4). However, note that Equation (12) is valid only for a limit point. The way we handle the situation in the case of a bifurcation point is explained in the next section.

3.2 Avoidance of bifurcation points

Ohsaki [19] explains thoroughly and systematically the computation of bifurcation point sensitivities; in particular he focuses on all possible difficulties, associated with this task. He also clearly states that a bifurcation point *usually* appears, if the structure possesses some kind of geometrical symmetry. This fact is exploited in the present work. Namely, to avoid the bifurcation nature of a critical point, the shape of the shell is perturbed by an asymmetric shape imperfection. This is motivated by the expectation that avoiding the bifurcation point is much more efficient then coping with the difficulties associated with it. It should be noted that an asymmetric shape imperfection does not guarantee the avoidance of a bifurcation point in all cases. However, numerical experiments show that a broad range of nonlinear structural optimization problems can be successfully solved by combining the procedure described in section 3.1 and the shape perturbation approach described below.

Let us consider, as an example, a symmetric bifurcation point. If the load factor decreases along the bifurcation path, see the solid line in Figure 3a, the bifurcation point is called a symmetric *unstable* bifurcation point. Otherwise, see the solid line in Figure 3b, it is called a symmetric *stable* bifurcation point. Note that for an unstable point, an asymmetric shape imperfection of the structure turns the bifurcation point into a limit point, see the dashed line in Figure 3a. An asymmetric shape imperfection also reduces the critical load factor. On the other hand, the symmetric stable bifurcation point vanishes when an asymmetric imperfection is induced, see the dashed line in Figure 3b. Thus, with an adequate asymmetric shape imperfection, most optimization problems, defined by Equations (4), can be solved quite efficiently.
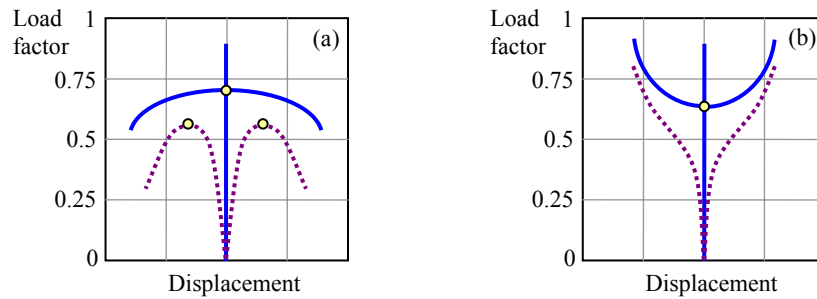

Figure 3. Equilibrium paths of a symmetric (solid) and asymmetrically perturbed (dashed) structure: (a) symmetric unstable bifurcation point and (b) symmetric stable bifurcation point.

Adequate asymmetric shape imperfection of the structure can be very efficiently achieved by utilizing the design element technique. For shell structures, the implementation of this technique is thoroughly discussed, e.g., in Reference [20]. The shape of the shell is controlled by the position of the control points, which in turn depend on the design variables. An example of a symmetric shallow shell, defined by a Bezier patch design element with 4×2 control points, is shown in Figure 4a. To optimize the shape of the shell, two design variables, b_1 and b_2, may be introduced as follows: $q_{21x} = -b_1$, $q_{21y} = b_2$, $q_{31x} = b_1$, and $q_{31y} = b_2$, where q_{21x} through q_{31y} are the control point positions, e.g. $\mathbf{q}_{21} = [q_{21x}, q_{21y}]^T$. Such an arrangement assures symmetric shape variation of the shell during the design process.
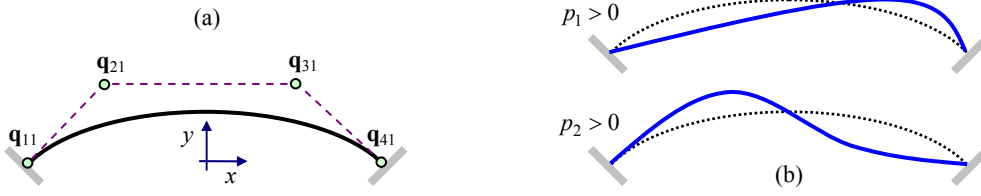
Figure 4. Shell (side view) with two variable control points: (a) symmetric design and (b) shape perturbations induced by p_1 and p_2, respectively.

To obtain an asymmetric shape perturbation, two imperfection parameters, p_1 and p_2, may be introduced by redefining the control point positions as follows: $q_{21x} = -b_1 + p_1$, $q_{21y} = b_2 + p_2$, $q_{31x} = b_1 + p_1$, and $q_{31y} = b_2 - p_2$. Non-zero values of p_1 and p_2 induce asymmetry to the shell, see Figure 4b. Thus, by utilizing the design element technique (or a similar approach), the imperfection parameters may be introduced into the model in the same manner as the design variables. Their introduction does not increase the complexity of the optimization process.

By implementing the above procedure, one can expect that for a broad range of problems the first critical point (if it exists) will be a limit point, when adequate values of the imperfection parameters are given. The next section discusses how to determine these values.

3.3 'Worst-case' asymmetric imperfection

Let all the imperfection parameters be assembled in the vector $\mathbf{p}$. When defining the values of its components, one has to find the ones which minimize the approximate critical load factor λ^*. This can be achieved by taking advantage of the iterative nature of the optimization process and by the fact that imperfection parameters are - from the technical point of view - of the same type as the design variables. Thus, $\mathbf{p}$ can be systematically improved during the optimization process by using the derivatives $d\lambda^*/d\mathbf{p}$. These derivatives can be readily obtained by the same part of the code that computes $d\lambda^*/d\mathbf{b}$, i.e. the expression for $d\lambda^*/d\mathbf{p}$ has the same structure as Equation (12).

$$\frac{d\lambda^*}{d\mathbf{p}} = \frac{\mathbf{y}^{*T}\left(\dfrac{\partial \mathbf{F}^*}{\partial \mathbf{p}} - \lambda^* \dfrac{d\mathbf{R}}{d\mathbf{p}}\right)}{\mathbf{y}^{*T}\mathbf{R}} \tag{13}$$

11

The improvement procedure is based on the assumption that the norm p of the vector $\mathbf{p}$ is a given data. By utilizing the derivatives $d\lambda^*/d\mathbf{p}$, the direction of $\mathbf{p}$ is gradually modified in order to get the lowest possible critical load factor, i.e., to get the 'worst-case' imperfection pattern. For this purpose, a simple gradient-projection method is used by which the imperfection parameters are updated as follows

$$\mathbf{p}^{k+1} = \xi^k \left(\mathbf{p}^k + \Delta\mathbf{p}^k \right), \quad \Delta\mathbf{p}^k = -\psi p \left(\frac{d\lambda^*/d\mathbf{p}}{\left\| d\lambda^*/d\mathbf{p} \right\|} \right)^k \tag{14}$$

where the superscript k denotes the current optimization iteration, $0 < \psi < 1$ is a parameter influencing the convergence, and ξ^k is a scaling parameter, assuring that $\left\| \mathbf{p}^{k+1} \right\| = p$. In our work, the convergence parameter was set to $\psi = 1/2$. The initial values $\mathbf{p}^{k=0}$ of imperfection parameters may be simply taken as $p_i^0 = p/\sqrt{N}$, $i = 1,\ldots,N$, where N denotes their total number.

Numerical experiments show that this simple optimization procedure generates a sequence $\mathbf{p}^k$, $k = 0,1,2,\ldots$, converging to some final value $\mathbf{p}^{opt}$. Obviously, in the space of imperfections, constrained by $\left\| \mathbf{p} \right\| = p$, $\mathbf{p}^{opt}$ represents a minimum point (at least a local one) of the critical load factor λ^*. Thus, assuming that the design variables also converge to some $\mathbf{b}^{opt}$, the final imperfection vector $\mathbf{p}^{opt}$ can be viewed as the 'worst-case' asymmetric shape imperfection pattern of the final design.

One can see that the imperfection parameters $\mathbf{p}$ are also optimized in some sense. Actually, the whole optimization procedure can be viewed as running two separate optimizations simultaneously, Figure 5. During the analysis phase, all the quantities, needed for both optimizations, are computed. If it turns out that the angle Φ between the vectors $\mathbf{y}^*$ and $\mathbf{R}$ is close to $\pi/2$, i.e. $\left| \cos\Phi \right| \leq 0.001$, the first critical point is assumed to be a bifurcation point. In this case, the imperfection variables are scaled by some predefined factor (e.g. $\mathbf{p}^{new} = 2\mathbf{p}$ seems to work fine) and the analysis is repeated until the product $\mathbf{y}^{*T}\mathbf{R}$ is far enough from zero. The analysis is followed by the optimization phase, which consists of two separate steps: *(i)* improvement of $\mathbf{p}$ by the simple update procedure, Equation (14), and *(ii)* improvement of $\mathbf{b}$ by a gradient-based optimizer. For the convergence check, both $\mathbf{b}$ and

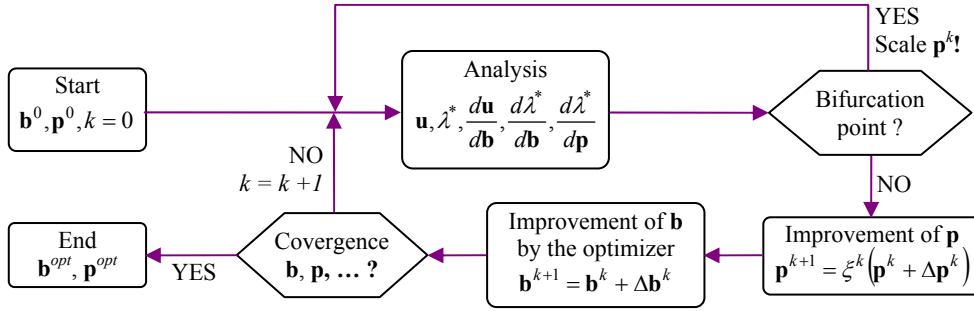**p** are taken into consideration, in addition to the objective and constraint functions.

Figure 5. The proposed optimization procedure.

3.4 Determination of imperfection amplitude

By the procedure from Figure 5, the imperfection pattern vector $\mathbf{p}^{opt}$ was obtained along with the optimal structural design. Assuming that the procedure was started with imperfections of a small amplitude and some scaling of $\mathbf{p}^{k}$ was necessary, the amplitude of $\mathbf{p}^{opt}$ may be roughly viewed as the lower amplitude limit, preventing the appearance of a bifurcation critical point. However, as noted e.g. by Mróz and Piekarski [6], the imperfection amplitude is also a very important parameter, being also related to structural cost. To account for this fact, it might be reasonable to optimize the amplitude of $\mathbf{p}$ as well. By adopting the suggestions of Reference [6], the imperfection amplitude parameter η is introduced, and the actual imperfection is now defined to be $\eta \mathbf{p}^{opt}$. To get the optimal η^{opt}, the optimization problem, Equations (4), is redefined as

$$\min\left(f_0^r + \frac{\omega}{\eta} \right)$$
$$s.t. \quad f_i^r \leq 0, \quad i = 1, \ldots, M \tag{15}$$
$$\lambda^* \geq 1 + \beta$$
$$\eta \geq \eta^{Low}$$

where η^{Low} is the lower limit of η and ω is a constant weighting factor, utilized to balance the importance of η with respect to the actual objective function f_0^r. This problem can now be solved for $\mathbf{b}^{opt,\eta}$ and η^{opt}, while the imperfection pattern $\mathbf{p}^{opt}$ is kept constant since the

design change $\mathbf{b}^{opt,\eta} - \mathbf{b}^{opt}$ is expected to be rather small. During this procedure, a bifurcation point may be encountered again. Although such a situation was not observed in numerical tests, it is still advisable to employ a procedure, proposed in Figure 6.
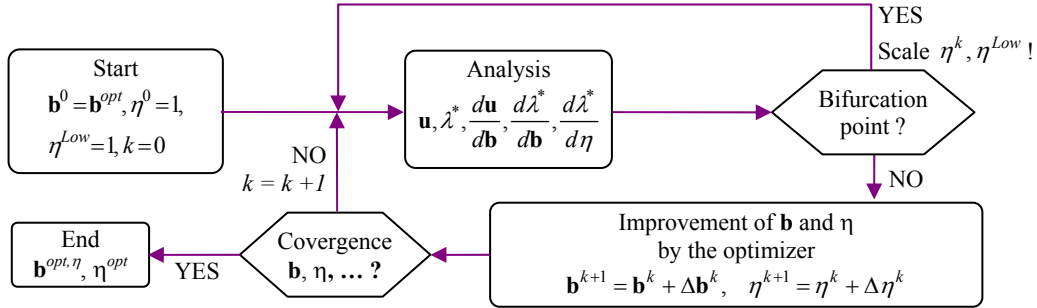

Figure 6. The procedure to get the imperfection amplitude.

4. Numerical examples

To illustrate the proposed approach, three numerical examples are considered. The first one presents an optimization of a shallow arch. It is a relatively simple problem, yet it exposes nicely all aspects of the considered topics. The second example considers a more complex shell structure with double curvature. The third example presents the optimization of truss-stiffened shell, which exhibits local buckling.

For the optimization of design variables $\mathbf{b}$, the gradient-based method, proposed in Reference [30], is used. This is a convex approximation method with automatically adjustable conservativeness. The automatic adjustments of the convex additive terms are based on the sensitivity information, collected during previous optimization steps.

For the response analysis, a nonlinear 4-node shell finite element is used, Reference [31]. Finite rotations are parametrized by a constrained rotation vector, Reference [32], which is consistent with the standard incremental solution schemes for nonlinear response analysis. Since it maintains additive rotational updates, it is also very suitable for optimization by gradient-based methods.

4.1 A shallow arch

The arch is depicted in Figure 7. Its dimensions are $a = 1000\,\text{mm}$ and $b = 100\,\text{mm}$. The thickness of the shell is design dependent; it is defined as $t = 20 + 10b_1\,\text{mm}$. The material is

linear elastic: Young's modulus is $E = 210000\,\text{MPa}$ and Poisson's ration is $\nu = 0.3$. The structure is loaded by a snow-like load $f = 2\,\text{MPa}$ in the negative y-direction. The arch is clamped at both ends.
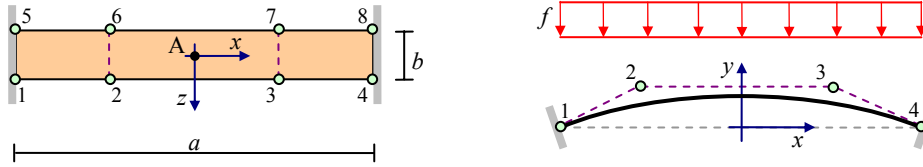

Figure 7.The shallow shell structure, defined by eight control points

To parameterize the shape of the structure, one design element with $4 \times 2 = 8$ control points is used. The control point (CP) positions are design dependent. Their definitions are given in Table I. One can see that three design variables, b_1 through b_3, are introduced. In addition, two imperfection parameters, p_1 and p_2, are incorporated into the CP positions, as illustrated in Figure 4.

The objective is to optimize the shape of the structure by minimizing its relative volume $v = V/V^{ini}$. The constraints are related to the apex point A. Its vertical position y_A is constrained by $y_A/y_{all} \leq 1$ and its vertical displacement u_{Ay} by $u_{Ay}/u_{all} \leq 1$. The allowable values are defined as $y_{all} = 50\,\text{mm}$ and $u_{all} = 10\,\text{mm}$. The initial design of the shell is given by $b_1 = b_2 = b_3 = 0$. At this design, the height of the arch is $y_A^{ini} = 37.5\,\text{mm}$.

To illustrate the difficulties of geometrically nonlinear structural optimization, three different approaches to optimal design were considered. First, we tried to solve the above optimization problem by using the conventional load-driven incremental (CLI) analysis. The perfect structure was considered, i.e. $p_1 = p_2 = 0$ was used for the response analysis. Since at the initial design the critical load level was $\lambda_{ini}^c = 0.903$, the structure buckled before the full load was reached. This resulted in failure of the optimization procedure already in the response analysis, due to the divergence in the Newton-Raphson procedure.

In the second attempt we performed the response analysis by the arc-length (AL) method, implemented in such a way that the equilibrium path was followed until the final load factor $\lambda = 1$ was reached. Now, the response analysis was always successfully completed, but the sequence of generated designs $\mathbf{b}^k$ alternated between stable (pre-critical state) and

15

unstable (post-critical state) designs, Figure 8a. At a stable design (denoted by a circle in Figure 8a), the constraints were generously fulfilled. This caused a design change, leading to an unstable structure (denoted by a square in Figure 8a) with heavily violated constraints. The consequence of excessive constraint violations was a recovery of a stable design. This scenario was then repeated sequentially.
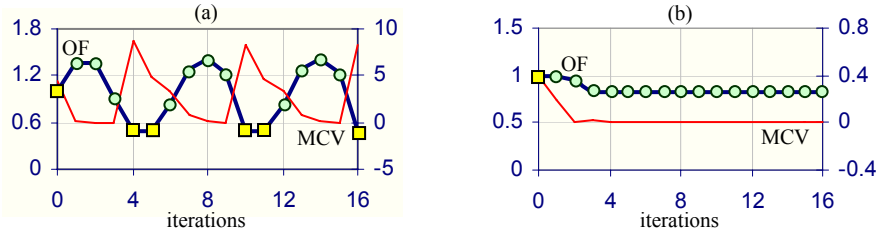

Figure 8. Iteration histories for the objective function (OF, left axis) and maximal constraint violation (MCV, right axis) of the arch: (a) the conventional approach (AL analysis) and (b) the proposed approach.

Finally, the constraint $\lambda^* \geq 1.2$ was added to the original optimization problem, as proposed in Section 3.1, and imperfections were introduced, as described in Sections 3.2 and 3.3. The starting values of the imperfection parameters were selected as $p_1^0 = p_2^0 = \frac{a}{1000} = 1$, so that $\|\mathbf{p}\| = \sqrt{2}$. The first response analysis was terminated at load factor $\lambda = 0.8$ (denoted by a square in Figure 8b). After that, full load carrying capability of the structure (denoted by a circle in Figure 8b) was recovered and the optimization process proceeded in a stable way, till the optimum design was obtained. At the optimal design, the constraints on y_A and λ^* were active. No scaling of the imperfection parameters was needed. Column 3 of Table II summarizes the results, where MCV denotes the maximal constraint violation.

To see the influence of imperfection parameters on buckling load, the critical load factor of the optimal structure was analysed with $p_1 = p_2 = 0$. With this setting, the critical load factor was obtained as 1.24 (note that the critical load factor of imperfect structure was 1.15, see Table II).

To verify the correctness of the computed imperfection parameters, the following optimization problem was solved

$$\min_{\mathbf{p}} \lambda^*_{\mathbf{b} = \mathbf{b}^{opt} = const.}, \quad \text{s.t.} \quad \|\mathbf{p}\| = \sqrt{2} \tag{16}$$

Note that the solution of this problem gives the 'worst-case' imperfection of the optimized

structure for the chosen imperfect parameters. A gradient-based optimization with respect to $\mathbf{p}$ was performed and the starting values were set to $p_1^0 = p_2^0 = 1$. The procedure converged very quickly (after a few iterations) to the solution $p_1^{opt} = 0.309$ and $p_2^{opt} = 1.380$. This is the same result as obtained by our update procedure, see Table II.

To get the optimal imperfection amplitude η^{opt}, the optimization problem was reformulated according to Equations (15) and solved for $\mathbf{b}^{opt,\eta}$ and η^{opt} by the procedure, given in Figure 6. Since the order of magnitude of v is unity, the weighting factor was taken to be $\omega = 0.1$. The optimization procedure run smoothly and no scaling of η^k, η^{Low} was necessary. The imperfection amplitude increased to $\eta^{opt} = 1.973$ which lead to an increase of the structural volume by 1.5%. The design change was rather minor, see columns 3 and 4 of Table II. Here it is worth to note that some other value of ω would yield another result. A larger weighting factor would yield larger allowable imperfection amplitudes, but the structural volume would also rise. Thus, the actual choice of ω depends strongly on the problem under consideration and can not be theoretically determined for the general case.

Finally, it is worth to get some insight into the sensitivity of the optimized structure, with respect to the imperfection amplitude. One can see from Figure 9 that the critical load factor decreases almost linearly when the imperfection amplitude increases beyond 3. In that range the dependency between η and the critical displacement is also practically linear. Thus, one can say that the optimized structure behaves in an expected way.
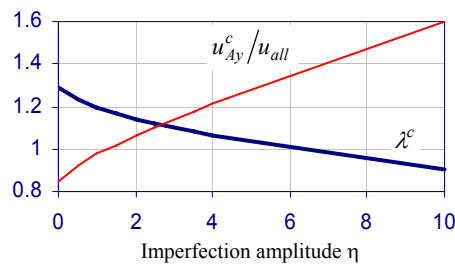

Figure 9. Critical load factor and the corresponding (normalized) critical displacement with respect to the imperfection amplitude.

4.2 A roof shell

The data of the structure are as follows. The distance $a = 20000\,\mathrm{mm}$ and the thickness

of the shells is $t = 100 + 50b_1$ mm. The material is linear elastic; Young's modulus is $E = 30000$ MPa, Poisson's ration is $v = 0.3$, and its density is $\rho = 4 \cdot 10^{-6}$ kg mm^{-3}. The structure is loaded by a snow-like load $f = 0.01$ MPa and its own weight. Both loads act in the negative y-direction. At all four corners the structure is pin-joined with fixed supports.

To parameterize the shape of the structure, one design element with $5 \times 5 = 25$ CP is used, Figure 10a. Their positions depend on 8 design variables b_2 through b_9. In addition, four imperfection parameters, p_1 through p_4, are incorporated into the definitions of CP positions, as shown in Figure 10b.

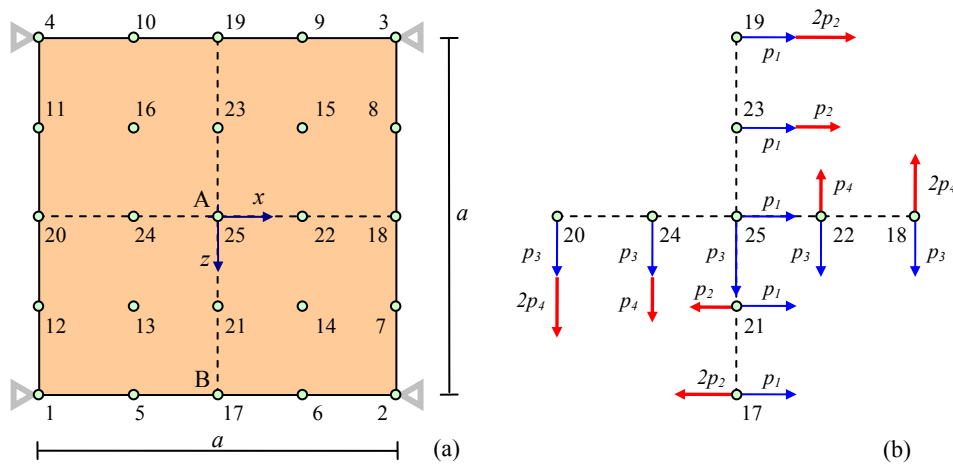

Figure 10.The roof shell structure: (a) groundplan with 25 CP and (b) influence of imperfection parameters on CP positions.

The objective is to optimize the shape of the structure by minimizing its relative volume $v = V/V^{ini}$. The constraints are related to the apex point A and point B, Figure 10a, as follows: $y_A/y_{all} \leq 1$, $u_{Ay}/u_{all} \leq 1$, and $u_{By}/u_{all} \leq 1$. The allowable values are defined as $y_{all} = 4000$ mm and $u_{all} = 10$ mm.

As in the first example, the conventional optimization procedure failed due to convergence problems during CLI response analysis of the perfect structure (at the starting design the critical load factor is $\lambda^c_{ini} = 0.76$). On the other hand, the employment of AL analysis resulted in extremely long computation times.
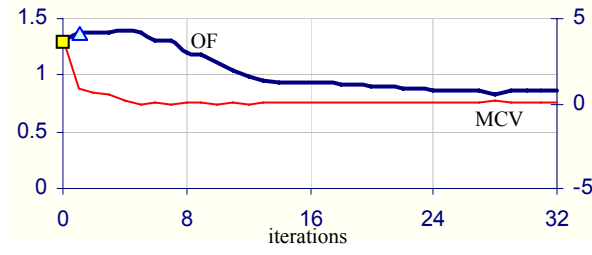
Figure 11. Iteration histories for the objective function (OF, left axis) and maximal constraint violation (MCV, right axis) of the roof shell.

By introducing the constraint $\lambda^* \geq 1.2$ and employing the procedure proposed in this paper, the problem was solved without difficulties. The initial imperfection parameters were set to $p_i^0 = \frac{a}{1000} = 20$, so that $\|\mathbf{p}\| = 40$. The first response analysis was terminated at load factor $\lambda = 0.6$ (denoted by a square in Figure 11). After the first iteration (denoted by a triangle in Figure 11), the first critical point became a bifurcation point. Therefore, the imperfection parameters were increased by a factor of 2, so that the norm of the imperfection vector was reset to $\|\mathbf{p}\| = 80$. After that, optimization proceeded normally with no further scaling of $\mathbf{p}$. At the optimal design, the constraints on y_A, u_{Ay}, and λ^* were active. The results are summarized in Table III and the optimal structure is shown in Figure 12. To see the influence of imperfection parameters, the critical load factor of the optimal structure was also analysed with $p_i = 0$. With this setting, the critical load factor raises from 1.21 to 1.27.
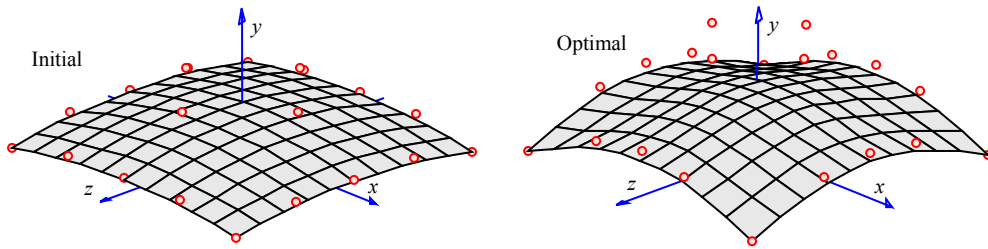

Figure 12. Initial and optimal design of the roof shell and the CP positions

To verify the correctness of the calculated imperfection parameters, the following optimization problem

$$\min_{\mathbf{p}} \lambda^*_{\mathbf{b}=\mathbf{b}^{opt}=const.}, \quad \text{s.t.} \quad \|\mathbf{p}\| = 80 \tag{17}$$

was solved by using gradient-based optimization. The starting values were set to $p_i^0 = 40$.

The procedure converged to the solution $p_1^{opt} = 80$ and $p_{2,3,4}^{opt} = 0$. This result is somewhat different than the one obtained by our update procedure, Table III. Closer analysis has shown that this is a consequence of the factor $\psi = 1/2$, used in the calculation of $\Delta \mathbf{p}^k$, Equation (14). To get a more accurate result, ψ should be gradually decreased towards zero when the optimization procedure converges towards $\mathbf{b}^{opt}$.

To get the optimal imperfection amplitude η^{opt}, the optimization problem given by Equations (15) was solved. The weighting factor was taken as $\omega = 0.1$. The optimization procedure run smoothly and no scaling of η^k, η^{Low} was necessary. The imperfection amplitude increased to $\eta^{opt} = 1.602$ which lead to an increase of the structural volume by 0.8%. From Table III it might seem that the design changes were rather significant. However, the design variables are mostly related to control point positions and the final structure, corresponding to $\mathbf{b}^{opt,\eta}$, looks practically the same as the optimal one, given in Figure 12.

Regarding the sensitivity of λ^c with respect to η, a similar observation can be made as in the first example, Figure 13. The critical displacement, however, behaves in a different way. At first u_{Ay}^c raises, but begins to decrease as η is increased beyond 4.
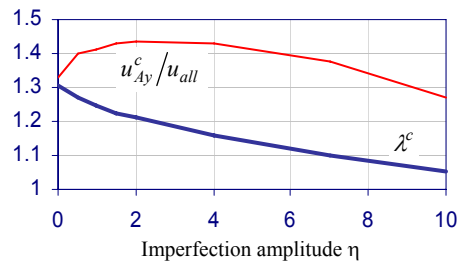

Figure 13. Critical load factor and the corresponding (normalized) critical displacement with respect to the imperfection amplitude.

4.3 A truss-stiffened shell

The structure consists of a quadrangular shell, pin-jointed with the upper layers of two slender truss-stiffeners, as shown in Figure 14a. Its dimensions are: $a = 6000\,\text{mm}$, $b = 750\,\text{mm}$, $c = 1500\,\text{mm}$. The thickness of the shell is $t = 10\,\text{mm}$. All bar elements are pipes with the outer radius equal to 15 mm and wall thickness of 1 mm. The material

properties are $E = 210000\,\text{MPa}$ and $v = 0.3$. The structure is loaded by a snow-like load $f = 0.01\,\text{MPa}$ in the negative z-direction. Both ends of the truss stiffeners are pin-joined with fixed supports.
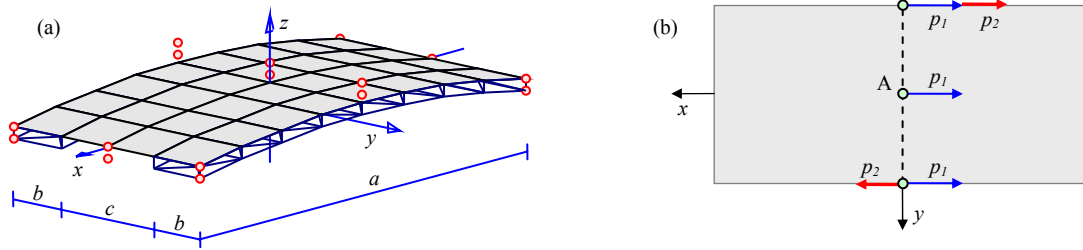

Figure 14. Truss-stiffened shell.

To parameterize the shape of the structure, one design element with $3 \times 3 \times 2 = 18$ CP is used, Figure 14a. Their positions depend on 4 design variables b_1 through b_4. In addition, two imperfection parameters, p_1 and p_2, are incorporated into the definitions of CP positions, as shown in Figure 14b.

The objective is to optimize the shape of the structure by minimizing its relative volume $v = V/V^{ini}$. The constraints are related to the vertical displacement of point A, Figure 14b, as follows: $u_{Az}/u_{all} \leq 1$ where $u_{all} = 50\,\text{mm}$.

When running the conventional optimization procedure with CLI response analysis, the convergence problems were not encountered although the structure buckled at several iterations. The reason was that the truss-stiffeners prevented global buckling of the structure and the shell buckled only locally in its middle region. So, there were no problems with the response analysis, but the optimization procedure yielded an oscillating sequence of solutions, some of them being stable and some of them being unstable, Figure 15a. Unstable structural designs are marked with squares in Figure 15a.
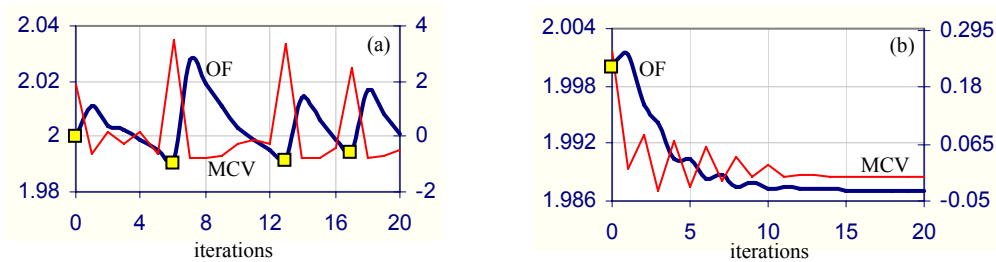

Figure 15. Iteration histories for the objective function (OF, left axis) and maximal constraint

violation (MCV, right axis): (a) the conventional approach (CLI analysis) (b) the proposed approach.

By introducing the constraint $\lambda^* \geq 1.2$ and employing the proposed procedure, the problem was solved without difficulties. The initial imperfection parameters were set to $p_i^0 = \frac{a}{1000} = 6$. The first response analysis was terminated at load factor $\lambda = 0.8$ (denoted by a square in Figure (15b)). After that, full load carrying capacity was recovered and kept throughout all iterations. No scaling of the imperfection parameters was needed. At the optimal design, the constraint on λ^* was active. The results are summarized in Table IV and the optimal structure is shown in Figure 16. To see the influence of imperfection parameters, the critical load factor of the optimal structure was also analysed with $p_i = 0$. With this setting, the critical load factor raises from 1.17 to 1.19.
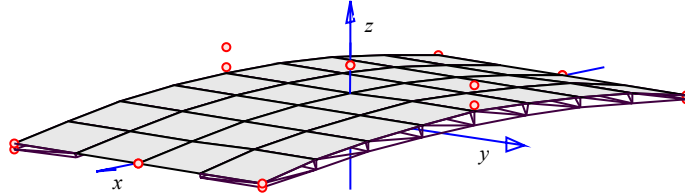

Figure 16. Optimal design of the truss-stiffened shell and the CP positions.

Conclusions

The paper presents an approach to optimization of stability-sensitive shell structures, subjected to displacement, stress, and similar constraints. Based on numerical experiments, the following conclusions can be made.

The proposed method offers a computationally inexpensive approach to optimization of stability-sensitive structures. Computational efficiency is assured by the following two points. Firstly, the critical states of the structure are never exactly computed, since the response analysis is always terminated prior reaching the first critical point. Only the conventional load-driven incremental response analysis is used. In addition, one eigenvalue/eigenvector pair has to be computed at each equilibrium point of the structural response. Secondly, the presence of bifurcation points is avoided by the introduction of imperfection parameters. This simplifies the sensitivity analysis of the critical load factor enormously and removes all the

inconveniences, associated with bifurcation points.

The imperfection parameters and the proposed update procedure reduce efficiently the imperfection sensitivity of the structure. After the 'worst-case' imperfection pattern is computed, its amplitude can be obtained within a few optimization cycles, utilizing a slightly altered optimization problem. Although the proposed technique works quite well, further improvements might be achieved by a more sophisticated update procedure. The introduction of another instance of the optimizer (one of them handling the design variables and the other one the imperfection parameters) might turn out to be of benefit. Another open question is the way how to introduce the imperfection amplitude into the objective function. Various choices produce various results and there seems to be no general guideline. Finally, quite important and still open questions relate to the choice of imperfection parameters - how many should be introduced, and how they should be related to the control point positions. These questions surely offer interesting topics of research, still to be done.

References

1. Kamat MP, Khot NS, Venkayya VB. Optimization of shallow trusses against limit point instability. *AIAA J.* 1984; 22: 403-408.

2. Khot NS, Kamat MP. Minimum weight design of truss structures with geometric non-linear behavior. *AIAA J.* 1985; 23: 139-144.

3. Saka MP, Ulker M. Optimum design of geometrically non-linear space trusses. *Comput. Struct.* 1992; 42: 289-299.

4. Reitinger R, Bletzinger KU. Shape optimization of buckling sensitive structures. *Comput. Systems Engng.* 1993; 5: 65-75.

5. Reitinger R, Ramm E. Buckling and imperfection sensitivity in the optimization of shell structures. *Thin-walled structures* 1995; 23: 159-177.

6. Mróz Z, Piekarski J. Sensitivity analysis and optimal design of non-linear structures. *Int. J. Num. Methods Engrg.* 1998; 42: 1231–1262.

7. Ohsaki M. Optimization of geometrically nonlinear symmetric systems with coincident critical points. *Int. J. Num. Methods Engrg.* 2000; 48: 1345–1357.

8. Ibrahimbegović A, Knopf-Lenoir C, Kučerova A, Villon P. Optimal design and optimal control of structures undergoing finite rotations and elastic deformations. *Int. J. Numer. Methods Engng.* 2004; 61: 2428-2460.

9. Kemmler R, Ramm E. Stability and large deformations in structural optimization. In Engineering Structures under Extreme Conditions (A. Ibrahimbegović, B. Brank, eds.), IOS, 2005, 312-328.

10. Wu CC, Arora JS. Design sensitivity of non-linear buckling load. *Comput. Mech.* 1988; 3: 129-140.

11. Park JS, Choi KK. Design sensitivity analysis of critical load factor for non-linear structural systems. *Comput. Struct.* 1990; 36 823-838.

12. Noguchi H, Hisada T. Sensitivity analysis in post-buckling problems of shell structures. *Comput. Struct.* 1993; 47: 699-710.

13. Mróz Z, Haftka RT. Design sensitivity analysis of non-linear structures in regular and critical states. *Int. J. Solids Struct.* 1994; 31: 2071–2098.

14. Ohsaki M, Uetani K. Sensitivity analysis of bifurcation load of finite dimensional symmetric systems. *Int. J. Num. Methods Engrg.* 1996; 39: 1707–1720.

15. Kemmler R, Lipka A, Ramm E. Large deformations and stability in topology optimization. *Struct. Multidisc. Optim.* 2005; 30: 459-476.

16. Samuelson LA, Eggwertz S. *Shell stability handbook*. Elsevier, 1992.

17. Wriggers P, Simo JC. A general procedure for the direct computation of turning and bifurcation points. *Int. J. Num. Methods Engrg.* 1990; 30: 155–176.

18. Planinc I, Saje M. A quadratically convergent algorithm for the computation of stability points: The application of the determinant of the tangent stiffness matrix. *Comput. Methods Appl. Mech. Engrg.* 1999; 169: 89-105.

19. Ohsaki M. Design sensitivity analysis and optimization for nonlinear buckling of finite-dimensional elastic conservative structures. *Comput. Methods Appl. Mech. Engrg.* 2005; 194: 3331-3358.

20. Kegl M, Brank B. Shape optimization of truss-stiffened shell structures with variable thickness. *Comput. Methods Appl. Mech. Engrg.* 2006; 195: 2611-2634.

21. Crisfield MA. *Non-linear Finite Element Analysis of Solids and Structures*. Wiley: New York, 1991.

22. Wu CC, Arora JS. Design sensitivity analysis and optimization of nonlinear structural response using incremental procedure. *AIAA J.* 1987; 25: 1118-1125.

23. Oblak MM, Kegl M, Butinar BJ. An approach to optimal design of structures with non-linear response. *Int. J. Num. Methods Engrg.* 1993; 36: 511-521.

24. Ohsaki M. Maximum loads of imperfect systems corresponding to stable bifurcation. *Int. J. Solids and Structures*. 2002; 39:927-941.

25. Ohsaki M, Uetani K, Takeuchi M. Optimization of imperfection-sensitive symmetric systems for specified maximum critical load. *Comput. Methods Appl. Mech. Engrg.* 1998; 166: 349-362.

26. Deml M, Wunderlich W. Direct evaluation of the 'worst' imperfection shape in shell buckling. *Comput. Methods Appl. Mech. Engrg.* 1997; 149: 201-222.

27. Wunderlich W, Albertin U. Analysis and load carrying behaviour of imperfection sensitive shells. *Int. J. Num. Methods Engrg.* 2000; 47: 255-273.

28. Belytschko T, Liu WK. B. Moran. *Nonlinear finite elements for continua and structures*. Wiley: New York, 2000.

29. Kwon TS, Lee BC, Lee WJ. An approximation technique for design sensitivity analysis of the critical load in non-liner structures. *Int. J. Num. Methods Engrg.* 1999; 45: 1727–1736.

30. Kegl M, Oblak MM. Optimization of mechanical systems: on non-linear first-order approximation with an additive convex term. *Commun. Numer. Methods Engrg.* 1997; 13: 13-20.

31. Brank B, Perić D, Damjanić FB. On implementation of a nonlinear four node shell finite element for thin multilayered elastic shells. *Computational Mechanics* 1995; 16: 341-359.

32. Brank B, Ibrahimbegović A. On the relation between different parametrizations of finite rotations for shells. *Engineering Computations* 2001; 18: 950-973.

Table I. Control point positions of the shallow arch

CP	X	Y	Z
1	-500	0	50
2	$-(200+200b_2)+p_1$	$(50+25b_3)-p_2$	50
3	$(200+200b_2)+p_1$	$(50+25b_3)+p_2$	50
4	500	0	50
5	-500	0	-50
6	$-(200+200b_2)+p_1$	$(50+25b_3)-p_2$	-50
7	$(200+200b_2)+p_1$	$(50+25b_3)+p_2$	-50
8	500	0	-50

Table II. Summary of results for the shallow arch

	Initial	Optimal	Optimal* ($\omega = 0.1$)
v	1.00	0.8249	0.8376
MCV	0.40	< 0.001	< 0.001
b_1; b_2; b_3	0; 0; 0	-0.354; -0.858; 0.667	-0.329; -0.873; 0.667
p_1; p_2	1; 1	0.309; 1.380	(0.309; 1.380)
λ^c; λ^*	0.90; 0.99	1.15; 1.20	1.14; 1.20
η	-	-	1.973

* Solution of Equations (15).

Table III Summary of results for the roof shell

	Initial	Optimal	Optimal* ($\omega = 0.1$)
v	1.00	0.8634	0.8701
MCV	3.87	< 0.001	< 0.001
b_1; b_2; b_3	0; 0; 0	-0.307; -0.243; -0.776	-0.295; -0.400; -0.699
b_4; b_5; b_6	0; 0; 0	-0.386; 1.458; 2.000	-0.138; 1.775; 2.000
b_7; b_8; b_9	0; 0; 0	-0.144; 0.845; 0.516	-0.344; 0.904; 0.376
p_1; p_2	20; 20	75.494; 3.125	(75.494; 3.125)
p_3; p_4	20; 20	24.815; 7.491	(24.815; 7.491)
λ^c; λ^*	0.76; 0.68	1.21; 1.20	1.25; 1.20
η	-	-	1.602

* Solution of Equations (15).

Table IV. Summary of results for the truss-stiffened shell

	Initial	Optimal
v	2.00	1.99
MCV	0.26	< 0.001
b_1; b_2; b_3; b_4	0; 0; 0; 0	1.0; 0.307; 1.0; -1.0
p_1; p_2	6; 6	-8.49; 0.00
λ^c; λ^*	0.94; 0.89	1.17; 1.20